Microstructural control during direct laser deposition of a β-titanium alloy

Qiu, Chunlei; Ravi, G.a.; Attallah, Moataz M.

DOI:
10.1016/j.matdes.2015.05.031

Document Version
Peer reviewed version

Citation for published version (Harvard):
Qiu, C, Ravi, GA & Attallah, MM 2015, 'Microstructural control during direct laser deposition of a β-titanium alloy', *Materials & Design*, vol. 81, pp. 21-30. https://doi.org/10.1016/j.matdes.2015.05.031

Microstructural Control During Direct Laser Deposition of a β-Titanium Alloy

Chunlei Qiu, G.A. Ravi, Moataz M. Attallah

PII: S0261-3069(15)00277-0
DOI: http://dx.doi.org/10.1016/j.matdes.2015.05.031
Reference: JMAD 7262

To appear in: *Materials and Design*

Received Date: 16 February 2015
Revised Date: 7 May 2015
Accepted Date: 8 May 2015

Please cite this article as: Qiu, C., Ravi, G.A., Attallah, M.M., Microstructural Control During Direct Laser Deposition of a β-Titanium Alloy, *Materials and Design* (2015), doi: http://dx.doi.org/10.1016/j.matdes.2015.05.031

Microstructural Control During Direct Laser Deposition of a β-Titanium Alloy

Chunlei Qiu, G. A. Ravi, and Moataz M. Attallah*

School of Metallurgy and Materials, The University of Birmingham, Edgbaston B15 2TT

Abstract

A concern associated with Direct Laser Deposition (DLD) is the difficulty in controlling microstructure due to rapid cooling rates after deposition, particularly in beta-Ti alloys. In these alloys, the beta-phase is likely to exist following DLD, instead of the desirable duplex alpha + beta microstructure that gives a good balance of properties. Thus, in this work, a parametric study was performed to assess the role of DLD parameters on porosity, build geometry, and microstructure in a beta-Ti alloy, Ti-5Al-5Mo-5V-3Cr (Ti5553). The builds were examined using optical microscopy, scanning electron microscopy, and X-ray diffraction. Microhardness measurements were performed to assess the degree of re-precipitation of alpha-phase following an in-situ dwelling and laser annealing procedure. The study identified several processing conditions that enable deposition of samples with the desired geometry and low porosity level. The microstructure was dominated by beta-phase, except for the region near the substrate where a limited amount of alpha-precipitates was present due to reheating effect. Although the microstructure was a mixture of equiaxed and columnar beta-grains alongside infrequent fine alpha-precipitates, the builds showed fairly uniform microhardness in different regions. In-situ dwelling and annealing did not cause an obvious change in porosity, but did promote the formation of alpha-precipitates.

Key words: Direct laser deposition; parametric study; beta-titanium alloys; build geometry; microstructure; microhardness

*Corresponding author: Tel: (+44) 121 414 7842; fax: (+44) 121 414 7890; e-mail addresses: m.m.attallah@bham.ac.uk (M.M. Attallah), c.qiu@bham.ac.uk (C. L. Qiu)

1. Introduction

DLD is an additive manufacturing technology that can be used to manufacture solid metallic components directly from a CAD (computer-aided design) file. During the process, powder is fed at a controlled rate into the laser focal point where it is melted into the melt pool. The path of the laser in the X-Y plane and along the Z axis is defined by a numerical control (NC) program which is derived from a CAD file of a component [1]. The technology has many potential applications, including production of functional prototypes, fabrication and repair of components, and fabrication of functionally graded materials and composites. Hybrid manufacturing using DLD is another potential application, whereby it can be used in combination with another manufacturing technology to deposit geometrical features in order to simplify the manufacturing process [2].

Compared to machining, DLD is particularly attractive for the fabrication of titanium aerospace components because it can greatly reduce the buy-to-fly ratio and lead-time for production; the two factors which impact the cost. Thus, a number of previous efforts have been undertaken to develop titanium DLD processes. Much of the focus of this prior research has been on α+β Ti-based alloys such as Ti-6Al-4V, Ti–6.5Al–3.5Mo–1.5Zr–0.3Si. Extensive study has been performed on these alloys in terms of structural integrity (e.g. porosity) [3-5], geometric integrity [3], microstructure [3-14], residual stress [15], distortion [3,15], mechanical properties and anisotropy [3,5,10,12] and the influence of laser processing condition and post-build heat treatment and hot isostatic pressing [3,5,16]. Throughout these studies, it is well understood that these alloys are liable to development of porosity especially lack-of-fusion pores at the inter-layer boundaries during DLD which are blamed for tensile anisotropy [3,5]. Also, these

alloys tend to develop columnar grains and strong texture after DLD [3,6,10,13].

In contrast, reports on DLD of β-Ti alloys such as Ti–25V–15Cr–2Al–0.2C, Ti-5Al-5Mo-5V-1Cr-1Fe and Ti-5Al-5Mo-5V-3Cr are rather limited, probably due to their relatively higher density and narrower applications as compared with α+β Ti-based alloys. There are only a few reports on DLD of β-Ti alloys so far, mainly focused on microstructural investigation. The influence of processing conditions on geometric integrity (such as build height and final shape) and porosity development of as-DLDed β-Ti alloys is not well understood. Wu et al. [17] studied the influence of DLD processing condition on the microstructure of Ti–25V–15Cr–2Al–0.2C and suggested that in contrast to Ti-6Al-4V the alloy formed equiaxed rather than columnar grains during DLD for a very wide range of processing conditions. They have attributed this to the unique solidification behaviour of this type of alloys which is dictated by their compositions. However, the variation trends in the grain structure between equiaxed grains and columnar grains with the processing parameters (such as laser power, scanning speed and powder feed rate) could still be observed for these alloys, suggesting that the thermal history, which is controlled by processing parameters, is another determining factor for the microstructural development in DLD. Liu et al [18] investigated the response of Ti-5Al-5Mo-5V-1Cr-1Fe to DLD and found that the as-fabricated microstructure contained a mixture of columnar grains and equiaxed grains which laid out in the form of a sandwich structure. They also recognised the inhomogeneous thermal distribution throughout the builds during DLD but did not investigate the microstructure in different regions (e.g. bottom up to top regions). Given that the microstructural development for β-Ti alloys is highly sensitive to thermal history and their α phase nucleation process is far more complicated than α+β Ti-based

alloys [19-21], it is necessary to examine the as-DLDed microstructures throughout the builds as the DLD process could cause different thermal effects in different regions.

Further, since the aerospace β-Ti alloys (e.g. Ti5553 and Ti-10-2-3) are typically forged and aged, their microstructure is typically composed of a α+β microstructure. Due to the rapid cooling rates associated with DLD, the microstructure is mostly composed of the β-phase, which does not necessarily achieve the required properties. Therefore, in the current study, in addition to the assessment of the impact of the process parameters on the geometry, structural integrity, microstructural and microhardness development during DLD of a β-Ti alloy (Ti5553), In-situ dwelling and annealing are also conducted with the aim of promoting the re-precipitation of the α-phase.

2. Experimental

The material used in this study was gas atomised Ti5553 powder supplied by TLS Technik, with a particle size range of 50-150μm. The particle size distribution of the as-received powder was analysed using both scanning electron microscope and a laser scattering particle size analyser and the result is shown in Fig. 1.

A 6.5-axis TRUMPF DLD (blown powder) system fitted with a 4 kW disc laser and an automatic spot change collimator (from 0.2 to 6mm) was used to deposit samples of dimensions $20 \times 20 \times 20$ mm^3. The setting up of this system has been described in detail elsewhere [1,3]. The NC program was created from the CAD file using ALPHACAM Mill software provided by Planit CAD/CAM Software, UK. Laser energy was delivered through an optical fibre into the

focal point formed on the substrate to which point powder was fed using a SIEMENS powder feeder through a 3 beam nozzle by argon. The desired spot size for the laser beam was achieved by varying the lens position automatically in the collimator.

The samples were deposited on thermomechanically processed and annealed Ti5553 substrates in an argon atmosphere to limit any oxidation, down to below 500 ppm prior to deposition. The substrates were cleaned and pre-heated with a high laser power. Samples were fabricated using a wide range of processing parameters, including different laser powers (1100-1600 W), scanning speeds (500-1100 mm/min), powder flow rates (4-9 g/min) and Z steps (0.5-1.0 mm). The actual parameters were normalised, as shown in Table 1. In-situ dwelling between the layers for 30 s and 60 s (with the laser beam switched off) and in-situ annealing at different laser powers (laser scan with no blown powder) at 200W and 400W were performed after each layer's deposition to assess their impact on the promotion of α-phase re-precipitation. In addition, the influence of in-situ dwelling and annealing on the structural integrity (porosity formation), microstructural, and microhardness development formation was also investigated. The detailed in-situ dwelling and annealing procedure and conditions are listed in Table 2. The deposition condition for this investigation was selected to be the Process condition 2 shown in Table 1.

The dimensions of the as-fabricated samples were measured in terms of their build heights. Because of the uneven surfaces, measurement of the build height was conducted on different locations of the sample surfaces, which gave rise to a range of build heights for each sample. Metallographic specimens were prepared and examined using optical microscopy (OM) to reveal the porosity size and distribution. Statistically representative images were taken and stitched to

develop a whole picture of a large section of the samples. Porosity level was evaluated by measuring the area fraction (A_f) of pores using Image-J software.

Samples were etched in an etchant containing 50 ml distilled water, 25 ml HNO_3 and 5 ml HF for microstructural characterisation using OM and a JEOL 7000 FEG scanning electron microscope (SEM). Electron Backscattered Diffraction (EBSD) was also conducted in the SEM to study the grain structure and X-ray diffraction was performed to identify the phases present following deposition. The EBSD samples used were polished and chemically etched in activated colloidal silica solution prior to EBSD examination. Finally, microhardness measurements were performed to trace the microhardness development along the build height using an Indentec Vickers microhardness testing machine using a 30kN load applied for 10 s.

3. Results

3.1 Influence of DLD processing condition on build height

Fig. 2(a) shows samples that were built using different processing conditions. It can be seen that the build height varies from one sample to another. The processing conditions together with the build height measurement results are listed in Table 1. It is obvious that the processing parameters, especially laser scanning speed and powder flow rate, have a significant influence on the build height and geometrical integrity. Thus, for Processes 1, 2, 3 where the Z step and powder flow rate are low and only the laser scanning speed is changed, a low laser scanning speed (Sp mm/min) was found to lead to a pronounced excess build (i.e. the actual build height is bigger than the specified height), whereas too high laser scanning speed such as (Sp+400) mm/min resulted in an under-build (i.e. the actual build height is lower than the program height).

The use of an intermediate scanning speed of (Sp+200) mm/min led to a good sample with a build height close to the specified height. At high laser power and high powder flow rate like Processes 8 and 9, lower scanning speed again led to excess build. The powder flow rate is also shown to demonstrate a remarkable influence on the build height; with other processing conditions being kept the same, increase of powder flow rate generally led to increase in build height. This is very obvious for Processes 3 and 4 where powder flow rate was increased by 1.7 g/min resulting in increase of build height by around 6 mm. Pronounced increase in build height was also observed from Process 7 to Process 8 (the latter shows higher powder flow rate). The dependence of build height on powder flow rate is clearly due to the fact that increased powder flow rate would allow more powder to be melted, which would increase the actual build layer thickness.

In contrast to laser scanning speed and powder flow rate, the laser power tends to show less influence on the build height when the other processing parameters are identical. Actually, an increase in laser power from P in Process 2 to (P+200) W in Process 6 did not lead to an obvious change to the build height. This also happened to Processes 3 and 5 where the difference in laser power did not change build height significantly either. This may be due to that P was already high enough to melt the captured powder and that further increase in laser power did not necessarily increase the powder capture rate and the amount of deposited materials within a specific duration.

The influence of Z-step on build height appears to depend on the actual build layer thickness. In Process 6, the Z-step 0.6mm is very close to the actual build layer thickness (around 0.62 mm)

and the total build height is close to the specified height whereas in Process 7, the Z-step is much bigger than the actual build layer thickness (which means the nozzle and the laser focal point would move further and further away from the build surface with continued building) and this would make the molten material splash off the build and lead to less material being deposited on the build surface and consequently to an under build. Similar phenomenon has been reported in Qiu et al's work on DLD of Ti-6Al-4V samples [3].

3.2 Influence of DLD processing condition on porosity and microstructure

Fig. 2(b-d) shows the porosity level of as-fabricated samples that were produced with process conditions 2, 6, and 8, all of which gave rise to the required geometry and build heights. It can be seen that all of these samples show low porosity (<0.1% in area fraction). Fig. 3 and Fig. 4 show the grain structure in the bottom and upper regions of the as-fabricated samples. All the samples showed a mixture of columnar grains and equiaxed grains. Detailed observation of the laser-melted beads revealed that each bead contains columnar grains at its peripheral regions and equiaxed grains in the centres. The columnar grains seem to have grown epitaxially between the layers. Also, it is noted that the bottom regions of the samples tend to be more dominated by columnar grains whereas the middle or top regions show increased numbers of equiaxed grains (Fig. 4). The difference in terms of grain structure is also illustrated using schematics (see Fig. 3(d) and Fig. 4(e)). Those columnar grains present in the upper regions also show reduced length and aspect ratio (length/width) as compared with those in the bottom region. This is consistent with Wu et al's work on DLD of Ti–25V–15Cr–2Al–0.2C [17]. Moreover, it can be seen that when other processing conditions were kept constant, increasing laser power (from Process 2 to Process 6) tends to generate more columnar grains and coarser grain structure; see Fig. 3(a-b)

relative to Fig. 4(a-b). However, when increasing laser power and powder flow rate simultaneously, the grain structure is almost unchanged; see Fig. 3(a) against Fig. 3(c).

The OM observation on grain structure was found to be consistent with SEM examination (see Fig. 5). Moreover, it was found that the bottom regions of the samples show considerable α-precipitation. This region was found to extend a maximum of 2 mm along the build direction. By contrast, the upper regions showed much less presence of α precipitates (Fig. 5(c-d)). The inhomogeneous α distribution was further verified by EBSD examination, as shown in Fig. 6(a) which shows phase distribution in a transitional region from α precipitates-rich region to upper region with much fewer α precipitates present. According to the EBSD result, the area fraction of α phase in the sample is around 0.5%. Fig. 6(b) shows the grain structure and orientations in this region. Again, a mixture of columnar grains and equiaxed grains could be observed.

Samples from different regions of a build were examined using XRD. The results are shown in Fig. 7. Only β-phase peaks are present, suggesting that the volume fraction of α phase is quite limited (<1%), both at the top and the bottom of the builds. This confirms the percent distribution as estimated with scanning electron microscopy.

Despite the heterogeneity in grain structure, the microhardness of the samples did not show a significant scatter throughout the samples, as shown in Fig. 8. Instead, all the samples show uniform and comparable microhardnesses (~ 280 HV). This is probably due to the fact that the grain size in the current samples is generally large (above 100μm) and an indent may have not covered sufficient grains.

3.3 Influence of in-situ dwelling and annealing on microstructure and microhardness

Fig. 9 shows the porosity level in the samples that had undergone in-situ dwelling and annealing. The porosity in all the samples is still very low (<0.1%), indicating that in-situ dwelling and annealing did not have considerable influence on porosity level and structural integrity of samples. However, the microstructure seems to be affected significantly. A heterogeneous microstructure was observed for all the samples, as shown in Fig. 10. A mixture of columnar and equi-axed grains could be observed throughout the samples. The upper regions generally show predominant β grains with only limited α precipitation. In contrast, the lower regions are almost dominated by α precipitates and laths. The morphology of α phase tends to vary with different processes probably due to the different thermal histories associated with different processing conditions and sequences (see Fig. 11). This kind of microstructure has led to a pronounced transition in microhardness from the lower regions to the upper regions (see Fig. 12). The lower regions generally show much higher microhardness as compared with the upper regions, probably due to the significant α precipitation.

4. Discussion

The current experimental results demonstrate that using a sufficient laser power, the build height and geometry are mainly affected by the laser scanning speed and powder flow rate. Thus, with other processing parameters being kept constant, the increase of either powder flow rate or laser scanning speed led to increase in build height. Powder flow rate actually defines the amount of powder that would be delivered to the laser focal point and melted by laser beam in a specific duration and thus would affect the actual layer thickness. Laser scanning speed affects the

amount of molten material that would be captured in a specific area. With lower scanning speed, it offers more time for material to drop onto a specific area on the build surface and there would be more material accumulation and build up, giving rise to thicker build layers. In contrast, laser power was found to show much less influence on build height as long as they are high enough to melt powder. This is obvious for Processes 2 and 6, and Processes 3 and 5 where increase of laser power did not lead to significant change in build height. This may be mainly due to the fact that the laser power did not affect significantly the powder capture rate and captured material once it is high enough to melt powder coming to the laser focus point. The influence of Z step on build height and quality totally depends on the deviation between the specified Z step and the actual building layer thickness. When the deviation is pronounced, the laser focal point would be further and further away from the build surfaces with increased build height. This would lead to change in powder capture rate and the amount of captured material and thus to the change in built layer thickness. This is consistent with previous work [3]. The results suggest that a proper combination of processing parameters is essential for successful building of samples with required geometry and height.

The current findings also demonstrate that with proper processing conditions, samples with good structural integrity (e.g. low porosity) could be achieved by DLD. Actually, the samples shown in Fig. 1 all show significantly low porosity level. The common planar or irregular-shaped pores which could easily form at the interfaces between adjacent layers due to lack of fusion during DLD of α+β Ti-based alloys [3-4] are not observed in the current alloy. This could be attributed to the use of high laser power and the good weldability of the current Ti5553 alloy, a single phase alloy. The as-fabricated samples were composed of a number of laser deposited beads each

of which shows a typical as-cast microstructure with columnar grains developed in their peripheral regions (i.e. top and bottom regions) and equiaxed grains in the centre, leading to a heterogeneous microstructure throughout the samples. The columnar grains were found to grow epitaxially from previous layer into the next layer, suggesting that the grains in the previous layer may have acted as nuclei for the development of crystals in the next layer. This process may have also been further driven by the preferred heat loss or cooling direction along the build down through the substrate. However, the columnar grains did not extend through a whole bead and instead equiaxed grains were formed in the centre, suggesting that the thermal gradient between the remaining melt and the columnar grains might have become small (which would impede the directional growth of columnar grains) and according to the classic solidification theory there may be a turbulent convection current in the liquid (which would help melt off tips or arms of the columnar grains and bring them into the liquid to act as seed crystals), both of which are essential for the formation of equiaxed grains in the bead centre [22]. The turbulent Marangoni convection current in the melt pool was possible during DLD given that the powder was blown by argon into the melt pool, bringing momentum and turbulence to the pool. With increased build height, the fraction and aspect ratio of columnar grains were found to decrease while the number of equiaxed grains increased. This is probably due to the fact that with increased build height and increased building time, both the substrate and build were getting hotter and hotter and thus the thermal gradient between the build and substrate and that within the build itself were getting increasingly reduced. This would impede the directional growth of columnar grains and promote the development of equiaxed grains. The influence of processing condition on grain structure was also noted. Thus, with other processing parameters being kept constant, increase in laser power (from Process 2 to 6) led to the coarsening of grains (see Fig. 2 (a,b) and Fig. 3(a,b)).

However, when the laser power was increased together with increased powder flow rate (see Processes 2 and 8), the grain structure show insignificant change as demonstrated in Fig. 2 (a) and (c). This is believed to be due to the fact that the increased powder flow rate would lead to more powder captured by the laser beam which requires more energy to get melted. As such, the increased fraction of energy due to the increased laser power may have been consumed in melting the additional captured powder rather than in promoting grain growth. The result suggests that other processing parameters such as powder flow rate could also affect the microstructural development. It is therefore concluded that the input energy density (which could be defined by laser power, scanning speed, powder flow rate, etc) and the thermal history may have determined the microstructural development and thus any processing parameter that would affect the energy density and thermal history may show influence on microstructure. This is consistent with previous studies [8,13,14,17] which also suggest that the microstructural development of Ti-alloys is highly dependent on thermal history. Another microstructural characteristic for the current as-fabricated Ti5553 samples is the precipitation of α phase at the very bottom region, which may be attributed to the continuous self-annealing effect due to heat sink down to the bottom region during fabrication. The current microstructural heterogeneity especially in grain structure was found not to cause pronounced scatter in microhardness throughout the samples, which could be simply due to the fact that the samples are generally dominated by β grains.

In-situ dwelling and annealing were found to lead to significant α precipitation in the lower regions in contrast to the predominant β grains in the upper regions. The reason for this microstructural transition is not fully understood but may be associated with the thermal histories

the samples had experienced. With in-situ dwelling and annealing, it offers more time for α precipitation to occur, particularly at the lower regions which are closer to substrate and experienced much more cooling cycles than the upper regions. The lower regions should have more chances to get to the ageing temperatures (around 600°C) which allows spur of α precipitation [19-20]. Due to the small size of the samples (final size is 20x20x20mm) and the use of high laser powers for deposition in the current study, the top regions have always been kept hot to remain as β phase. The separated microstructures in the lower and upper regions have led to a pronounced transition in microhardness between the two regions. The lower regions showed much higher microhardness obviously due to the predominance of α phase.

Future work will focus on more comprehensive mechanical evaluation through tensile, fatigue and crack propagation tests to understand the mechanical response of the as-fabricated microstructures. Particularly, since the current samples generally contain a mixture of columnar and equiaxed grains and the samples fabricated with in-situ dwelling and annealing even show different microstructures in different regions of the samples, it is necessary to identify the weak link within the heterogeneous microstructure as well as to find out the mechanical consistency/scatter in these samples. These will be studied by performing both tensile and fatigue tests and by investigating the fracture surfaces and longitudinal sections of tested specimens (to study the primary and secondary cracking). In-situ synchrotron X-ray imaging will be performed to study the crack and damage development within these samples. These will help reveal the scatter in mechanical properties as well as identify the crack initiation sites and fracture mechanism of the as-fabricated microstructures. TEM (transmission electron microscopy) experiments will be performed on tensile tested samples to study the deformation behaviours (dislocation structure) of different microstructural features, particularly to reveal whether

heterogeneous deformation has happened within the heterogeneous microstructure.

5. Conclusions

This study showed that DLD can be optimised to achieve the required build height and low porosity in Ti5553 samples. When the laser power is high, the build height mainly depends on the laser scanning speed and powder flow rate; further increase in laser power did not affect build height obviously but did lead to coarsening of grain structure with other processing parameters constant. However, under this condition, the microstructure is heterogeneous, containing a mixture of columnar grains and equiaxed grains. The as-fabricated samples were dominated by β-phase grains except for the bottom regions of the samples where considerable α precipitates were present. This work identified the benefit of using in-situ dwelling without laser scanning and in-situ laser annealing to promote α precipitation in the lower regions of the samples, which led to improved microhardnesses that are close to that of forged Ti5553.

Acknowledgements

The work shown in this paper was financially sponsored by Messier-Bugatti-Dowty, Safran Group.

References

[1] Ravi GA, Hao XJ, Wain N, Wu X, Attallah MM. Direct laser fabrication of three dimensional components using SC420 stainless steel. Mater Des 2013;47:731-6.

[2] Martina F, Williams SW, Colegrove P. Improved microstructure and increased mechanical properties of additive manufacture produced Ti-6Al-4V by interpass cold rolling**.** 2013 Annual International Solid Freeform Fabrication Symposium - An Additive Manufacturing Conference**,** Austin, Texas, USA, pp. P490-6. Available on line with the link: http://sffsymposium.engr.utexas.edu/Manuscripts/2013/2013-38-Martina.pdf.

[3] Qiu CL, Ravi GA, Dance C, Ranson A, Dilworth S, Attallah MM. Fabrication of large Ti–6Al–4V structures by direct laser deposition. J Alloys Comp 2015;629:351–61

[4] Kobryn PA, Moore EH, Semiatin SL. The effect of laser power and traverse speed on microstructure, porosity, and build height in laser-deposited Ti-6Al-4V. Scripta Mater 2000;43: 299-305

[5] Kobryn PA, Semiatin SL. Mechanical Properties of Laser-Deposited Ti-6Al-4V. Solid Freeform Fabrication Symposium Proceedings, Austin, 2001, 179-86

[6] Kobryn PA, Semiatin SL. Microstructure and texture evolution during solidification processing of Ti–6Al–4V. J Mater Proc Tech 2003;135:330-9

[7] Wu X, Liang J, Mei J, Mitchell C, Goodwin PS, Voice W. Microstructure of laser-deposited Ti-6Al-4V. Mater Des 2004;25:137-44

[8] Brandl E, Michailov V, Viehweger B, Leyens C. Deposition of Ti–6Al–4V using laser and wire, part I: Microstructural properties of single beads. Surf Coat Tech 2011;206:1120-9

[9] Brandl E, Palm F, Michailov V, Viehweger B, LeyenS C. Mechanical properties of additive manufactured titanium (Ti–6Al–4V) blocks deposited by a solid-state laser and wire. Mater Des 2011;32:4665-75

[10] Carroll BE, Palmer TA, Beese AM. Anisotropic tensile behavior of Ti–6Al–4V components fabricated with directed energy deposition additive manufacturing. Acta Mater 2015;87:309–20

[11] Zhu YY, Liu D, Tian XJ, Tang HB, Wang HM. Characterization of microstructure and mechanical properties of laser melting deposited Ti–6.5Al–3.5Mo–1.5Zr–0.3Si titanium alloy. Mater Des 2014;56:445–53

[12] Zhu YY, Liu D, Tian XJ, Li J, Wang HM. The anisotropy of laser melting deposition additive manufacturing Ti–6.5Al–3.5Mo–1.5Zr–0.3Si titanium alloy. Mater Des 2015;67:538–42

[13] Zhu YY, Liu D, Tian XJ, Li J, Wang HM. Microstructure evolution and layer bands of laser melting deposition Ti–6.5Al–3.5Mo–1.5Zr–0.3Si titanium alloy. J Alloys Comp 2014;616:468–74

[14] Wang T, Zhu YY, Zhang SQ, Tang HB, Wang HM. Grain morphology evolution behavior of titanium alloy components during laser melting deposition additive manufacturing. J Alloys Comp 2015; 632: 505–513

[15] Denlinger ER, Heigel JC, Michaleris P, Palmer TA. Effect of inter-layer dwell time on distortion and residual stress inadditive manufacturing of titanium and nickel alloys. J Mater Proc Tech 2015;215:123–31

[16] Lu Y, Tang HB, Fang YL, Liu D, Wang HM. Microstructure evolution of sub-critical annealed laser deposited Ti–6Al–4V alloy. Mater Des 2012;37:56-63

[17] Wu X, Sharman R, Mei J, Voice W. Microstructure and properties of a laser fabricated burn-resistant Ti alloy. Mater Des 2004;25:103-9

[18] Liu CM, Tian XJ, Tang HB, Wang HM. Microstructural characterization of laser melting deposited Ti–5Al-5Mo–5V–1Cr–1Fe near β titanium alloy. J Alloys Comp 2013;572:17–24

[19] Boyne A, Wang D, Shi RP, Zheng Y, Behera A, Nag S, Tiley JS, Fraser HL, Banerjee R, Wang Y. Pseudospinodal mechanism for fine a/b microstructures in b-Ti alloys. Acta Mater 2014;64:188–97

[20] Nag S, Banerjee R, Srinivasan R, Hwang JY, Harper M, Fraser HL. ω-Assisted nucleation and growth of a precipitates in the Ti–5Al–5Mo–5V–3Cr–0.5Fe β titanium alloy. Acta Mater 2009;57:2136–47

[21] Jones NG, Dashwood RJ, Jackson M, Dye D. β Phase decomposition in Ti–5Al–5Mo–5V–3Cr. Acta Mater 2009;57:3830–9

[22] Porter PA, Easterling KE. Phase transformations in metals and alloys. 2nd edn. London: Chapman & Hall; 1992, p. 233-6.

Table 1 Processing conditions and dimensions of the as-fabricated Ti5553 samples

Processing condition or Sample Number	**Z step (mm)**	**Average Laser power (W)**	**Scan speed (mm/s)**	**Powder flow rate (g/min)**	**Expected height (mm)**	**Actual build height (mm)**	**Excess or under build or Good**
1	**0.6**	**P**	**Sp**	**F**	**9**	**12.4-13.7**	**Excess**
2	**0.6**	**P**	**Sp+200**	**F**	**20**	**21-22**	**Good**
3	**0.6**	**P**	**Sp+400**	**F**	**20**	**16.5-17.5**	**Under**
4	**0.6**	**P**	**Sp+400**	**F+1.7**	**20**	**22.7-24.3**	**Excess**
5	**0.6**	**P+200**	**Sp+400**	**F**	**20**	**16-17**	**Under**
6	**0.6**	**P+200**	**Sp+200**	**F**	**20**	**20.2-22**	**Good**
7	**0.8**	**P+200**	**Sp+200**	**F**	**20**	**14.6-16.6**	**Under**
8	**0.8**	**P+200**	**Sp+200**	**F+1.7**	**20**	**20.3-23**	**Good**
9	**0.8**	**P+200**	**Sp+100**	**F+1.7**	**20**	**23-25.4**	**Excess**

P is a laser power between 1200-1400W, S_p is a laser scanning speed between 500-700mm/min, F is a powder feed rate between 5.0-7.0g/min.

Table 2 In-situ dwelling and annealing procedure and conditions

	Processing procedure and condition
D30	Deposition + Dwell for 30s with laser off at each layer
D60	Deposition + Dwell for 60s with laser off at each layer
DA200	Deposition + Dwell 30s with laser off at each layer + Anneal 200W at each layer +Dwell 30s with laser off at each layer +Deposition……
DA400	Deposition + Dwell 30s with laser off at each layer +Anneal 400W at each layer +Dwell 30s with laser off at each layer +Deposition……

Figure Captions

Fig. 1 (a) Back-scattered electron SEM image of the as-received Ti-5553 powder particles and (b) particle size distribution analysed by a laser scattering particle size analyser

Fig. 2 (a) The as-fabricated Ti-5553 builds; (b-d) OM micrographs for the builds showing the reduced porosity in the builds, (b) Sample 2, A_f = 0.01%; (c) Sample 6, A_f = 0.02%; (d) Sample 8, A_f = 0.02%.

Fig. 3 OM micrographs showing the grain structure at the bottom regions of different builds, (a) Sample 2; (b) Sample 6; (c) Sample 8; (d) Schematics showing the typical grain structure at the bottom regions of the as-DLDed samples. The broken lines show the boundaries of re-melted zones.

Fig. 4 OM micrographs showing the grain structure in the upper regions of different samples, (a) Sample 2; (b) Sample 6; (c-d) Sample 8; (e) Schematics showing the typical microstructure in the upper regions of the as-DLDed samples. The dash lines show the boundaries of re-melted zones.

Fig. 5 Secondary electron SEM micrographs for the typical microstructure in the Ti5553 builds at (a-b) bottom region; (c-d) upper region.

Fig. 6 (a) EBSD phase map showing the distribution of α and β phases in transition region; (b) EBSD image showing the dominant β-grain structure; (c) the inverse pole figure for the β grain structure. The arrow shows the building direction.

Fig. 7 XRD patterns of an as-DLDed sample from bottom region and upper region

Fig. 8 Microhardnesses of as-fabricated Ti-5553 samples along build height, showing (a) sample 2; (b) sample 6; and (c) sample 8

Fig. 9 OM micrographs showing the as-polished samples that had been subjected to in-situ dwelling and annealing during DLD, (a) sample D30; (b) sample D60; (c) sample DA200; and (d) sample DA400.

Fig.10 Typical microstructure of samples that experienced in-situ dwelling and annealing during DLD, (a) photograph showing the etched samples with pronounced contrast between the upper regions and lower regions; (b) secondary electron SEM image showing the upper regions are dominated by β-grains; (c-d) secondary electron SEM image showing the lower regions are rich of α precipitates and laths.

Fig. 11 Secondary electron SEM micrographs showing microstructure of the lower regions of samples that had underwent different in-situ dwelling and annealing processes; (a) sample D30; (b) sample D60; (c) sample DA200; and (d) sample DA400.

Fig. 12 Microhardnesses of the builds subjected to in-situ dwelling and annealing along build height; (a) sample D30; (b) sample D60; (c) sample DA200; and (d) sample DA400.

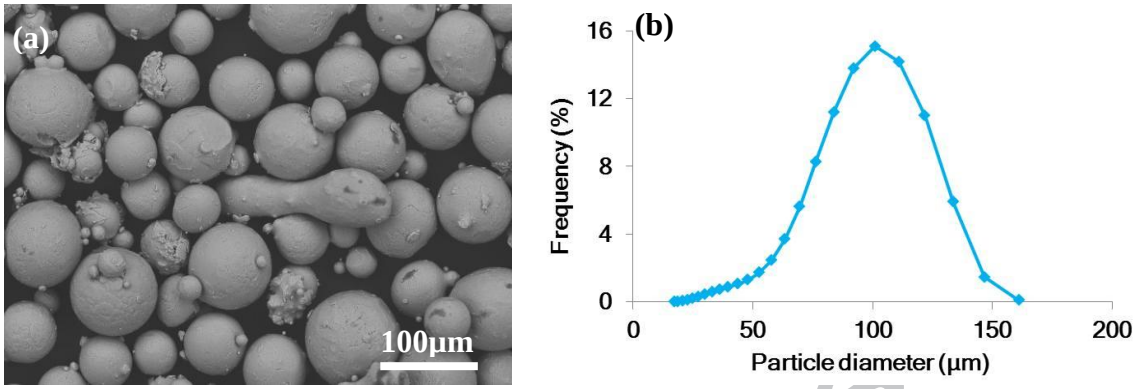

Fig. 1

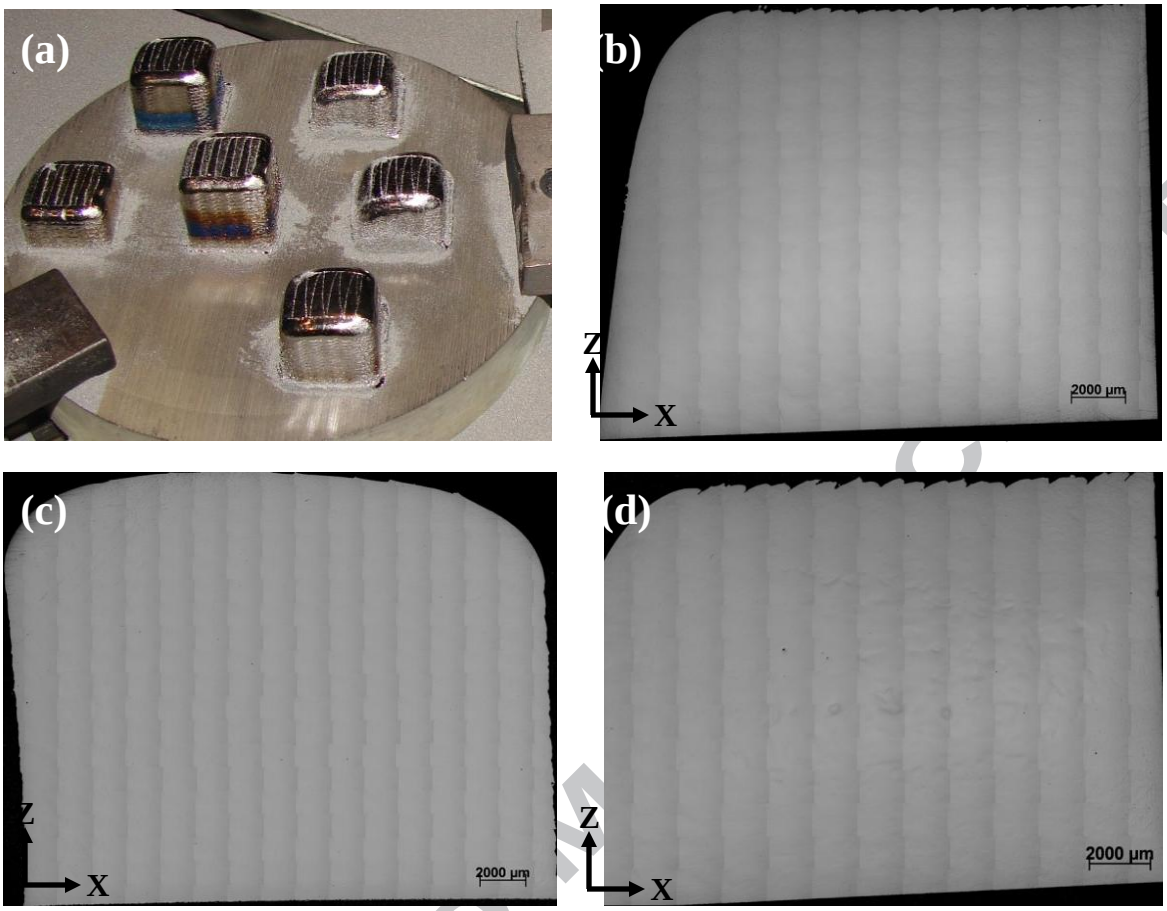

Fig. 2

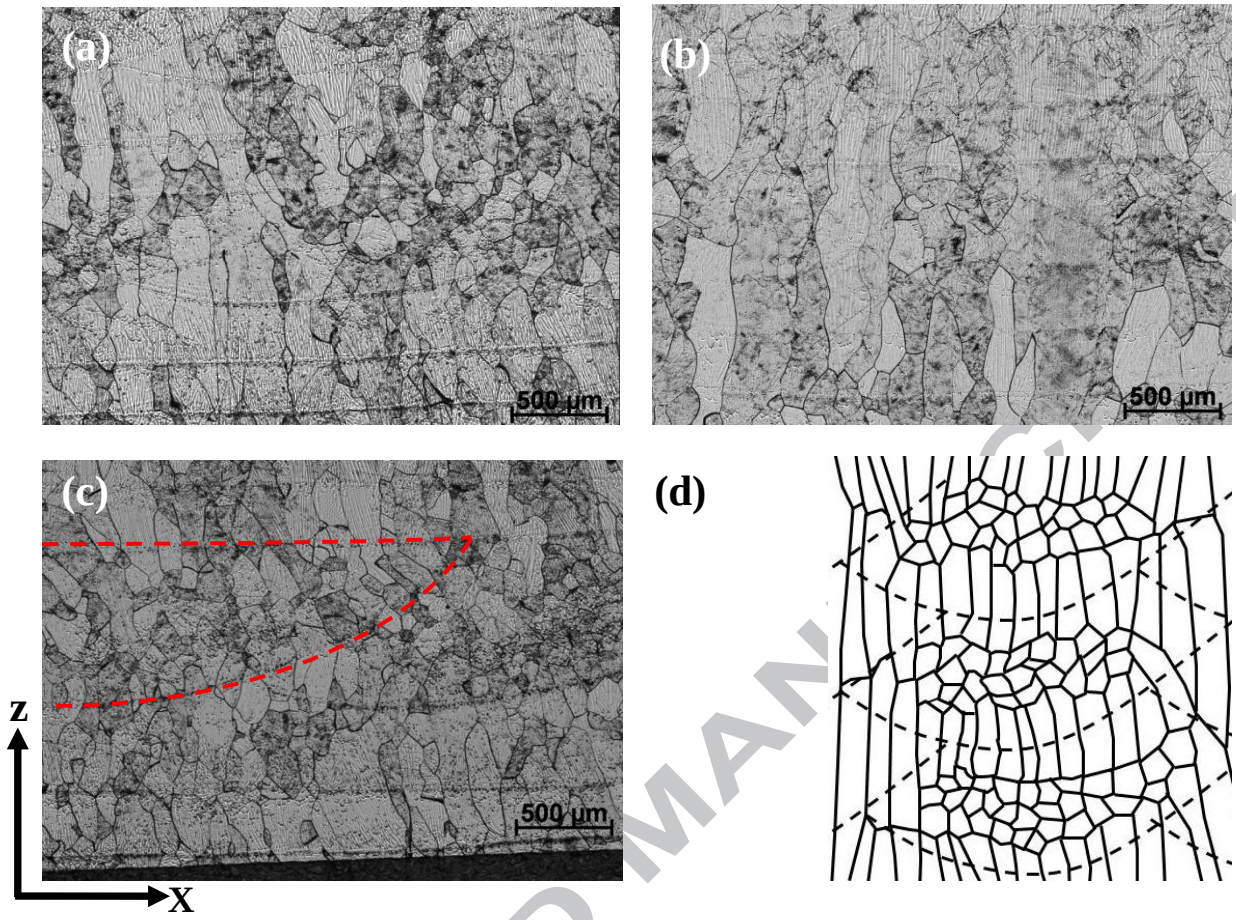

Fig. 3

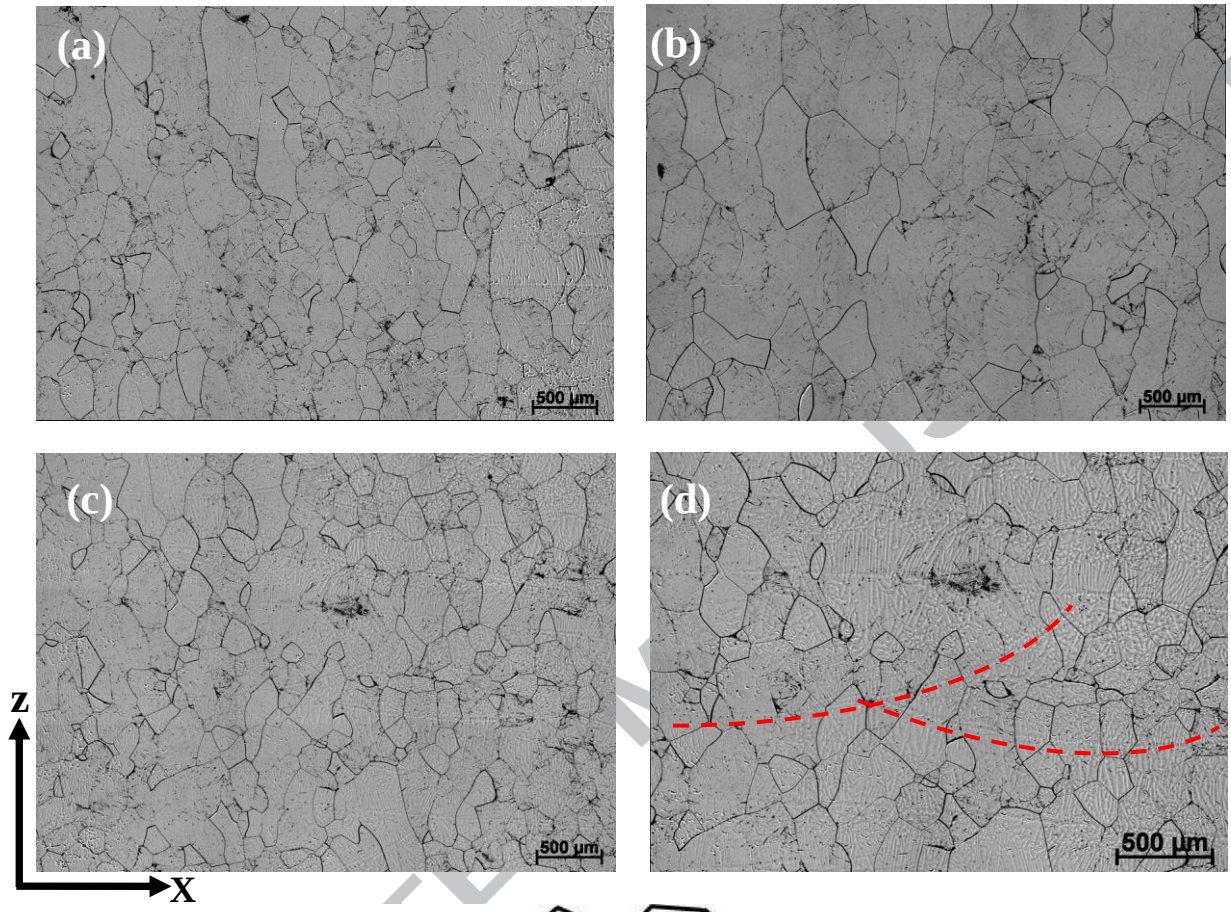
(a)
500 µm
(b)
500 µm
(c)
500 µm
(d)
500 µm
Z
X

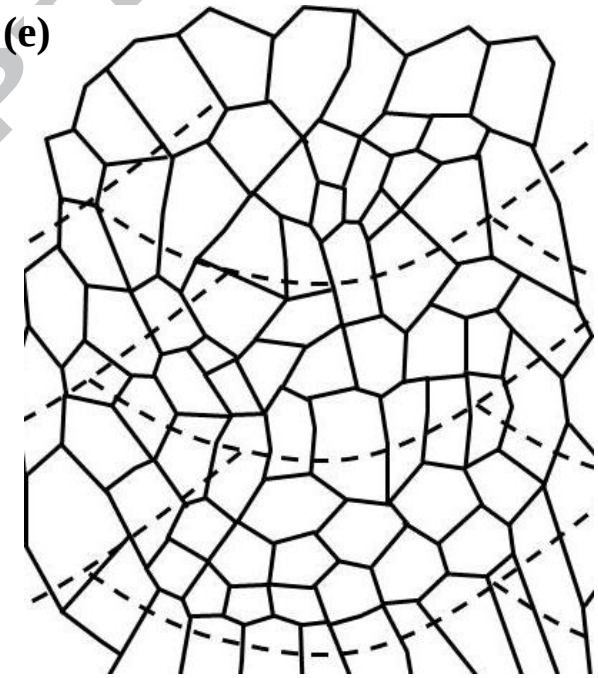
(e)

Fig. 4

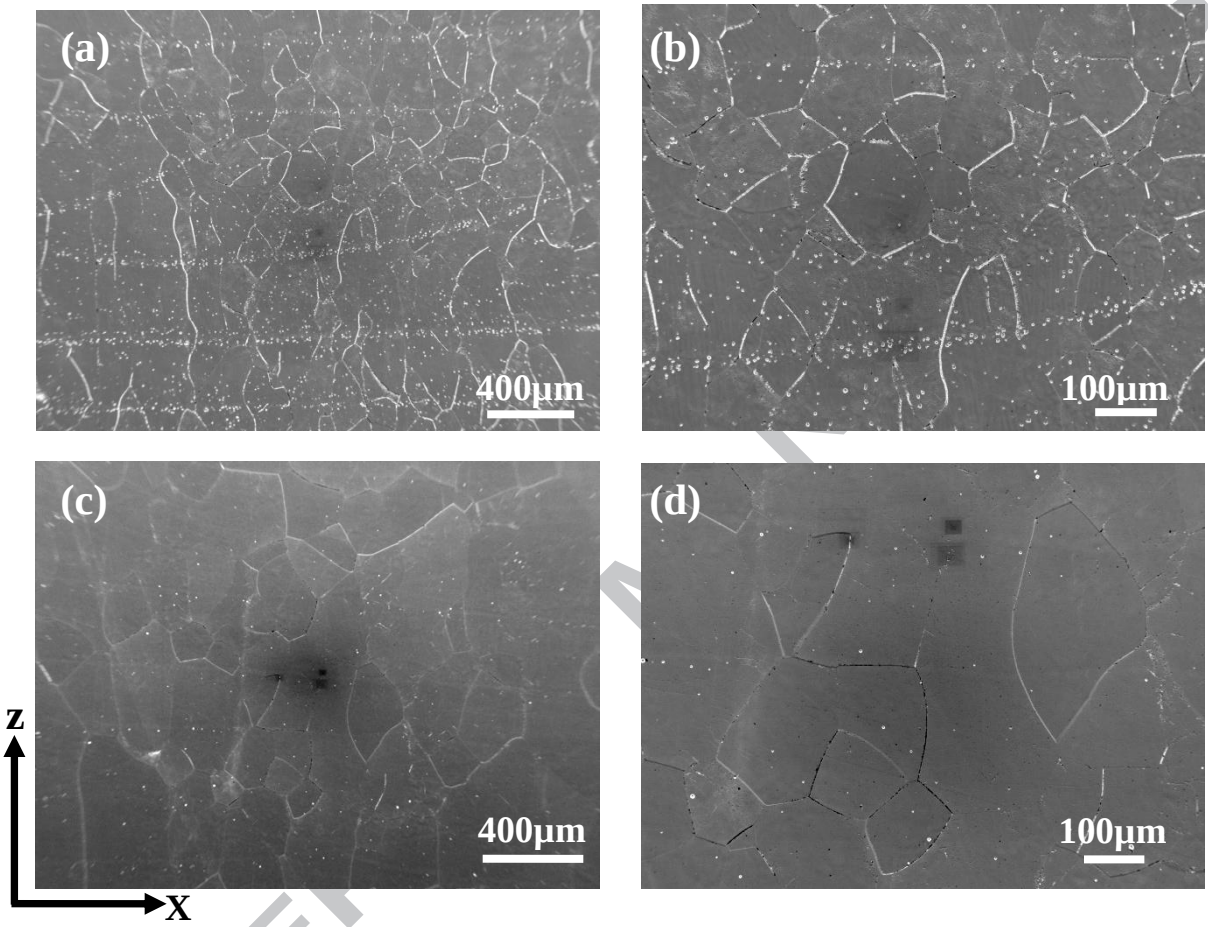

Fig. 5

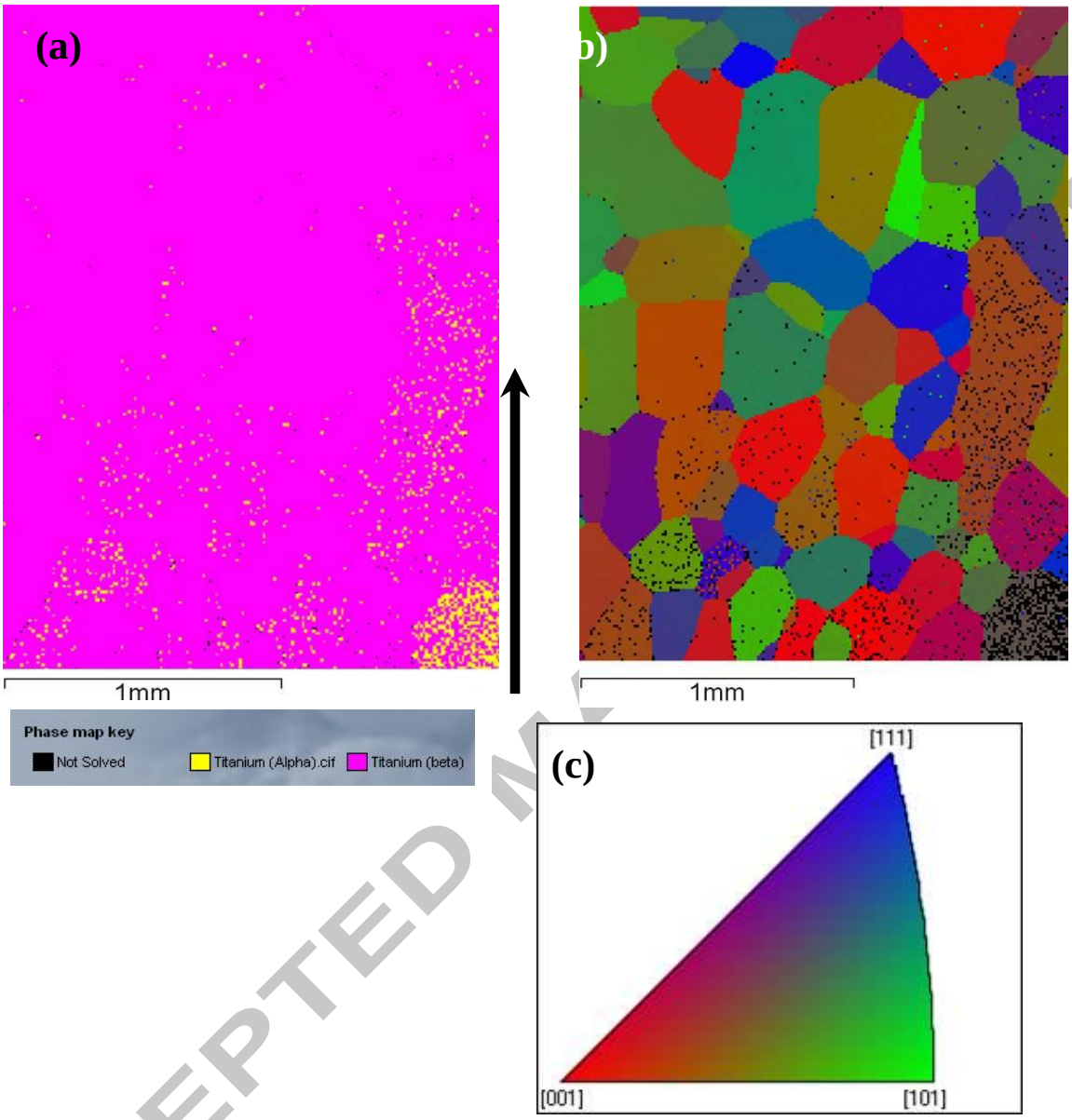

Fig. 6

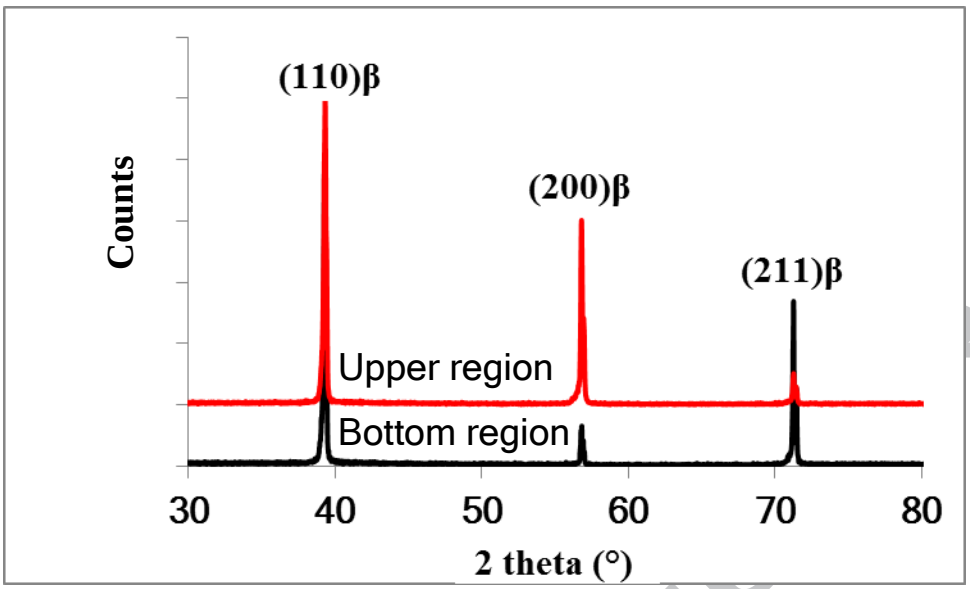

Fig.7

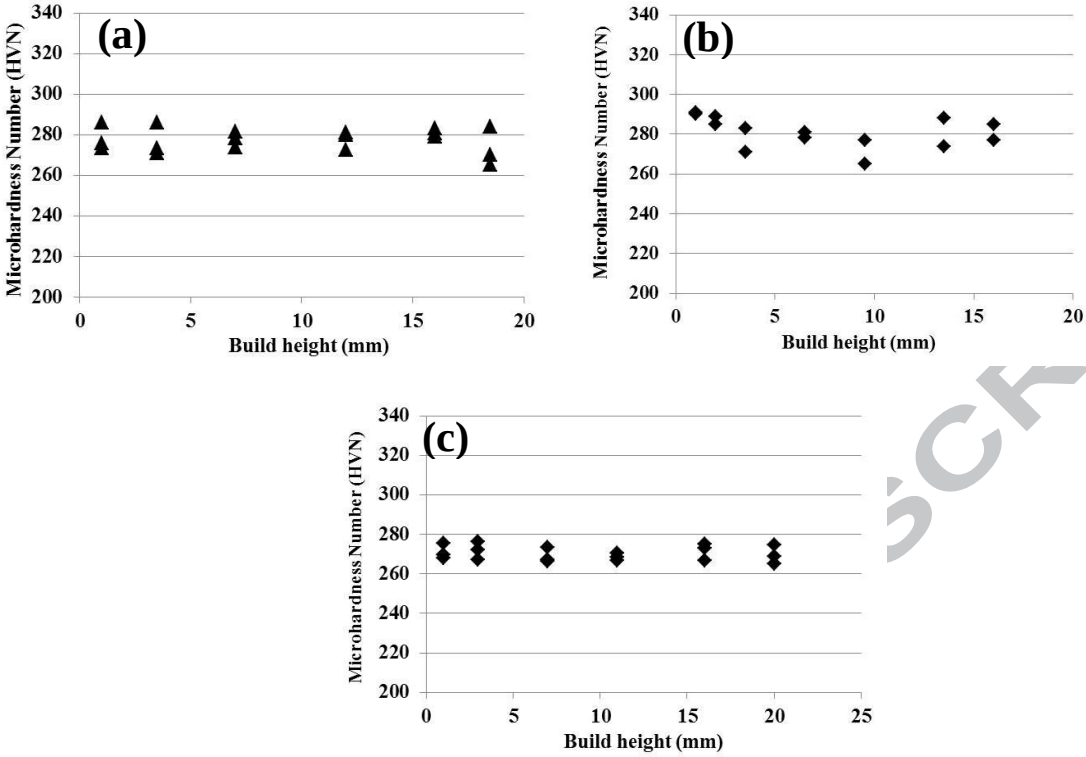

Fig. 8

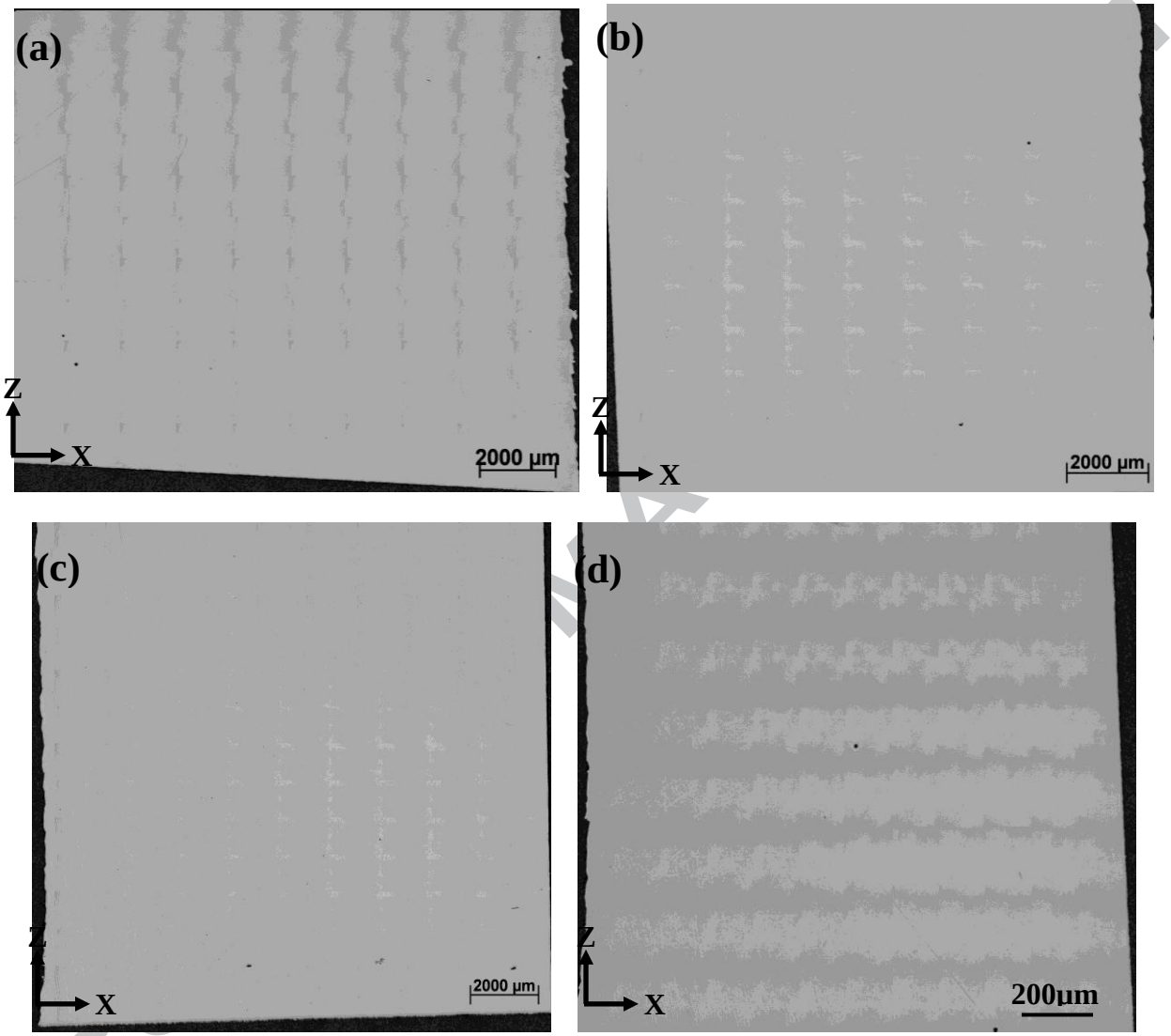

Fig.9

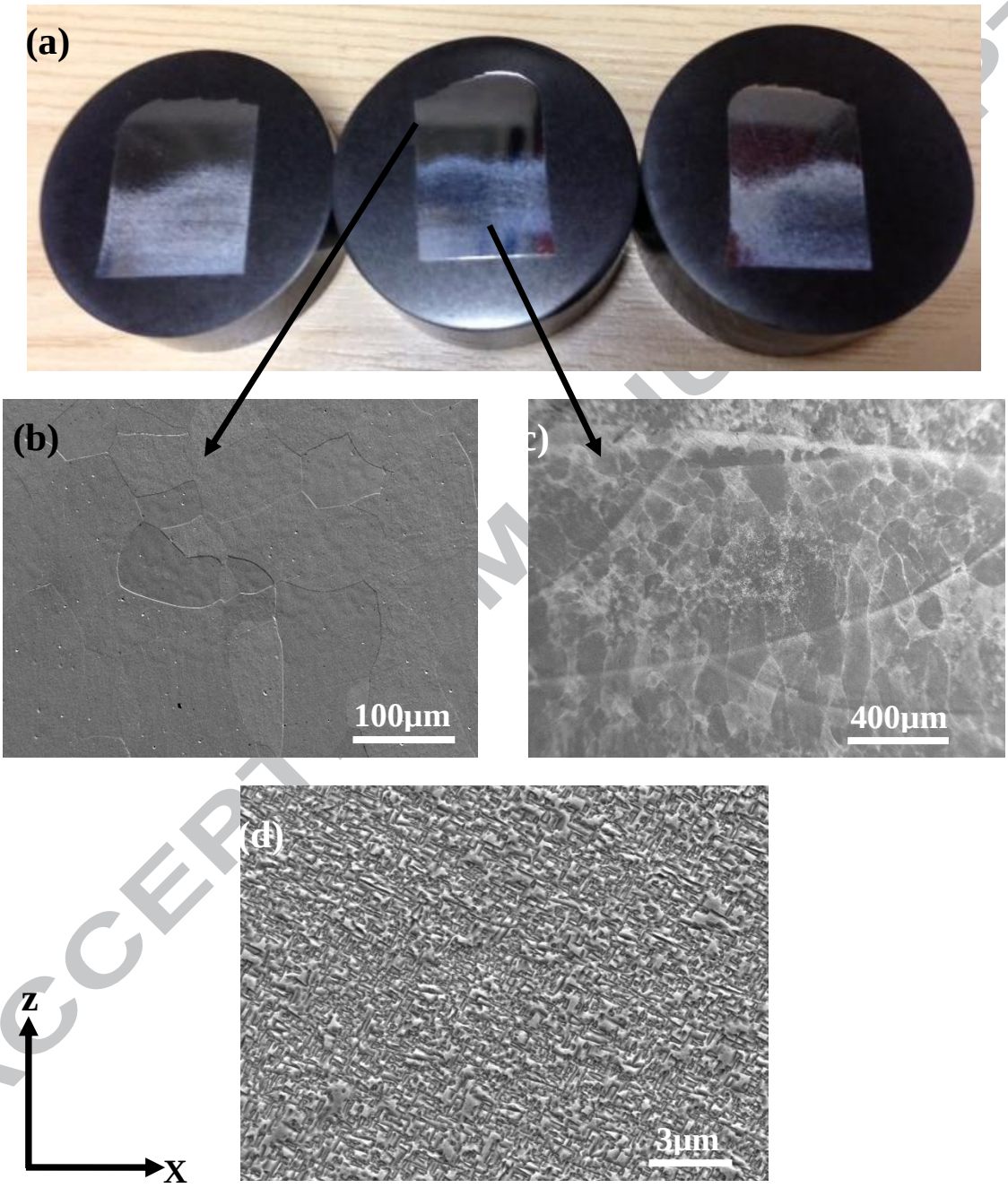
(a)
(b)
100µm
(c)
400µm
(d)
3µm
z
X

Fig. 10

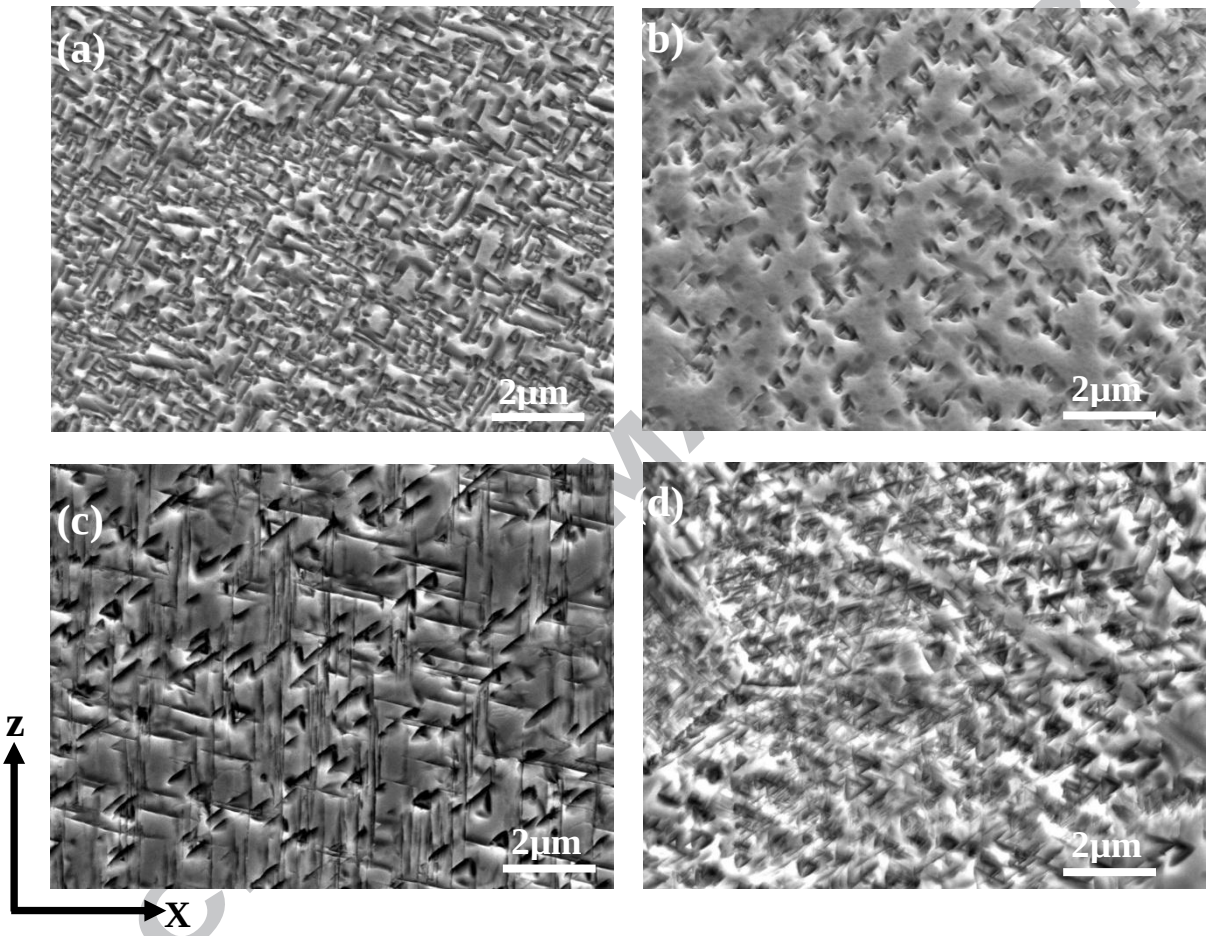

Fig. 11

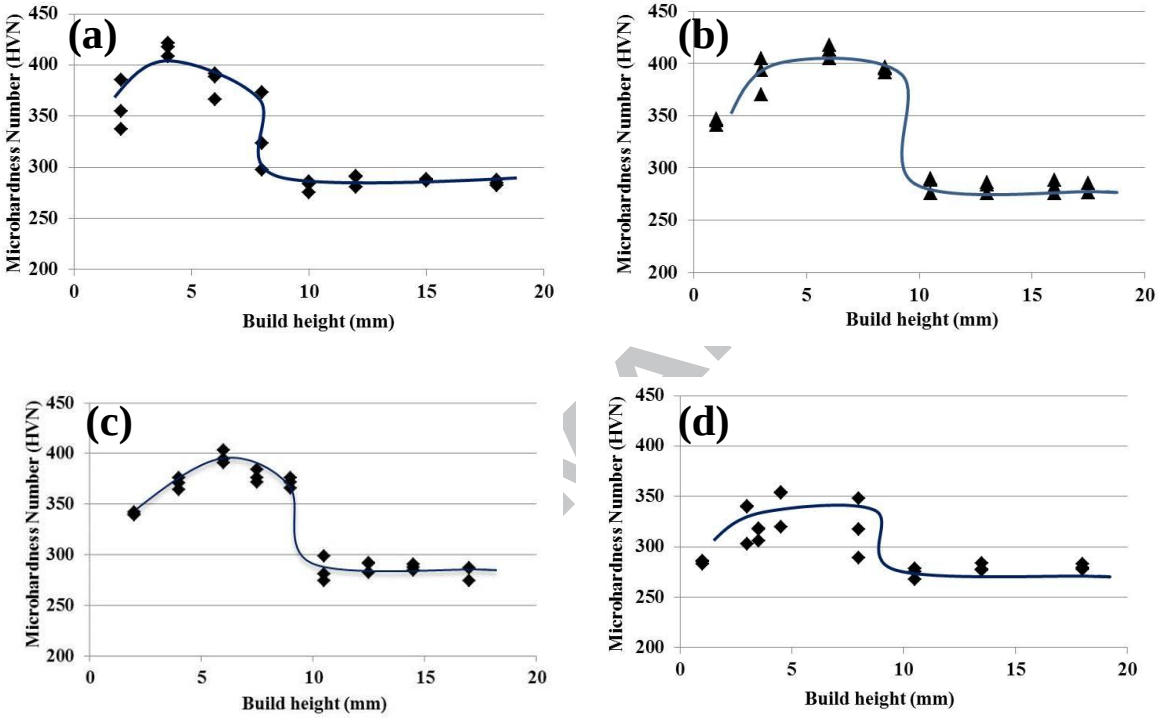

Fig. 12

Graphical Abstract

Microstructural development of Ti5553 during direct laser deposition (DLD)

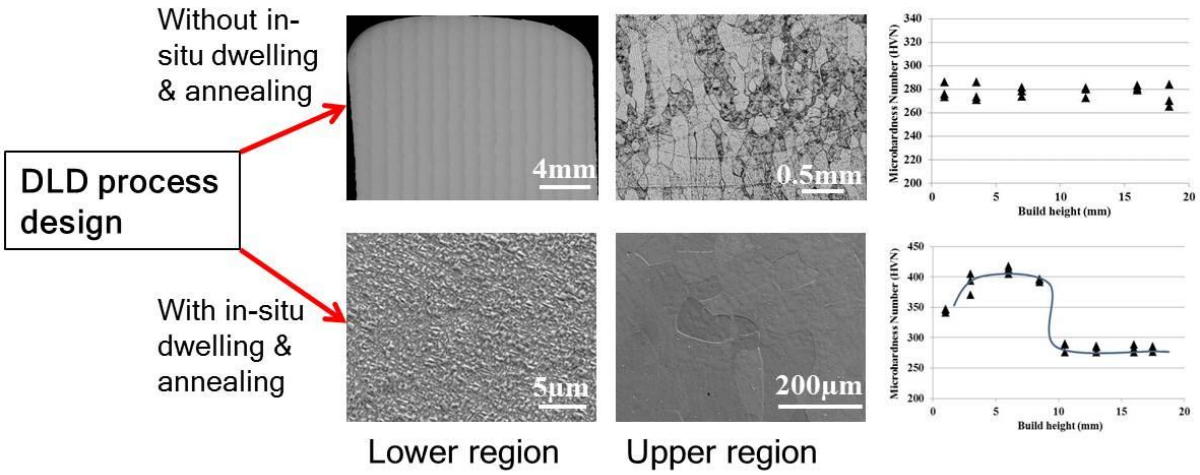

Research Highlights

- DLD process design leads to the acquisition of low porosity and required build height
- Build height increases with decreased scanning speed and increased powder flow rate
- Keeping Z step close to the actual layer thickness is crucial for consistent building
- The as-DLDed Ti5553 are dominated by mixed columnar and equiaxed grains
- In-situ dwelling and annealing promote α precipitation which improves microhardness